ORIGINAL ARTICLE



Modeling of nonlinear viscous damper response for analysis and design of earthquake-resistant building structures

Baiping Dong¹ · Richard Sause² · James M. Ricles²

Received: 2 March 2021 / Accepted: 10 December 2021

© The Author(s), under exclusive licence to Springer Nature B.V. 2021

Abstract

Studied are the hysteretic force-deformation response of large-scale nonlinear viscous dampers and model of the response for use in numerical simulations and seismic design. The force–deformation response of nonlinear viscous dampers with a force capacity of 600 kN are characterized under sinusoidal loading. A wide range of amplitudes and frequencies are used in the characterization tests. A nonlinear Maxwell model is presented for modeling the force-deformation response of large-scale nonlinear viscous dampers for use in nonlinear response history analyses. This paper also presents an equivalent linear model for the force-deformation response of a nonlinear viscous damper in-series with the elastic bracing and connection components needed to connect the damper to a building structure. The equivalent linear model enables the effects of the elastic flexibility of structural components on the response of the damper-brace component to be considered in seismic design. Results from tests on a 0.6-scale three-story structure with nonlinear viscous dampers validated the predictive accuracy of the equivalent linear model. Also evaluated are the effects of the elastic flexibility of structural components (e.g., bracing and connection) on the effective stiffness and damping ratio of a building structure with nonlinear viscous dampers.

Keywords Nonlinear viscous damper · Nonlinear Maxwell model · Structural flexibility · Effective stiffness · Equivalent damping ratio · Seismic design

☐ Baiping Dong baipingdong@tongji.edu.cn

Published online: 21 January 2022

Richard Sause rs0c@lehigh.edu

James M. Ricles jmr5@lehigh.edu

ATLSS Engineering Research Center, Department of Civil and Environmental Engineering, Lehigh University, Bethlehem, PA 18015, USA



State Key Laboratory of Disaster Reduction in Civil Engineering, Tongji University, Shanghai 200092, China

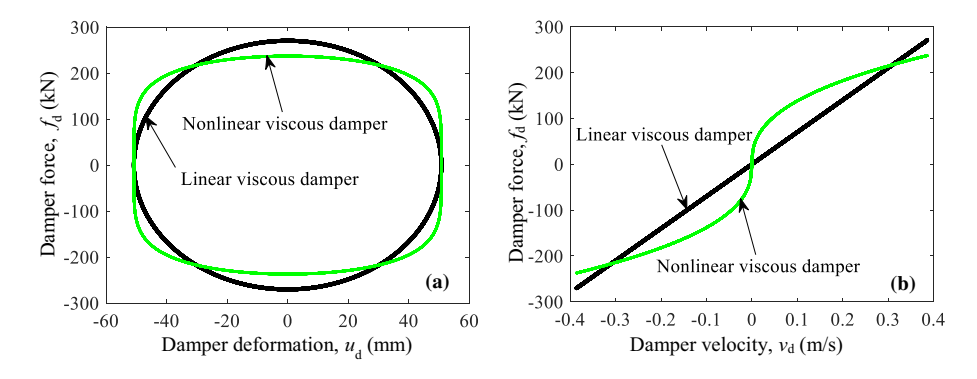
1 Introduction

Research (e.g., Soong and Spencer 2002; Christopoulos and Filiatrault 2006; Symans et al. 2008; Dong et al. 2016, 2018) has shown that viscous dampers have the potential to significantly improve the seismic response of building structures by adding damping and reducing inelastic deformation demands on the primary Seismic force-resisting system (SFRS) of structures under earthquake shaking. The theoretical force-deformation relationship for typical fluid viscous dampers is:

$$f_{\rm d} = C_{\alpha} \cdot \operatorname{sgn}(v_{\rm d}) \cdot |v_{\rm d}|^{\alpha} \tag{1}$$

where $f_{\rm d}$ is the damper force; $v_{\rm d}$ is the relative velocity across the damper (i.e., the rate of the damper deformation $u_{\rm d}$); ${\rm sgn}(v_{\rm d})$ is the direction of the relative velocity across the damper, where ${\rm sgn}(v_{\rm d})=1$ for $v_{\rm d}\geq 0$ and ${\rm sgn}(v_{\rm d})=-1$ for $v_{\rm d}<0$; C_{α} is the damping coefficient; and α is the velocity exponent. Linear viscous dampers have the value of α equals to 1.0, while nonlinear viscous dampers have the value of α less than 1.0. Figure 1 illustrates the difference in damper force–deformation response between linear and nonlinear viscous dampers. It can be seen that the nonlinear viscous damper has a smaller maximum damper force than the linear viscous damper for the same damper deformation and equivalent energy dissipation (i.e., equal-area hysteresis loops). Therefore, an equally effective nonlinear viscous damper in energy dissipation as a linear viscous damper would generate a smaller damper force amplitude, which is favorable in seismic design to reduce stress and deformation in adjacent structural components.

Both the NEHRP Recommended Seismic Provisions FEMA P-750 (BSSC 2009) and the building code ASCE/SEI 7–16 (ASCE 2016) have included provisions for seismic design of structures with passive damping devices. In these provisions, a damping device is defined as a flexible structural element that dissipates energy due to relative motion between each end of the device. In developing a realistic force–deformation model for a damping device, the pins, bolts, gusset plates, braces, brace extensions, and other components required to connect the damping device to the seismic mass of the building structure should be considered. Based on which, a damping system is defined as a structure with damping devices and all the structural components that transfer forces from the damping device to the seismic mass of the structure and the base of the structure.



 $\textbf{Fig. 1} \ \ \textbf{Theoretical hysteretic response of viscous damper: a damper force-deformation response; b damper force-velocity response$



The effects of the elastic flexibility of the structural components on the efficiency of dampers in structures for supplemental damping and reduction of earthquake induced structural response have been broadly discussed in literature. Sause et al. (1994) revealed the dependence of near-optimal damping for viscoelastic damper on brace stiffness and demonstrated that the increase in the brace stiffness increases the level of damping and reduction of seismic response of viscoelastic-damped frame structures. Fu and Kasai (1998) demonstrated that the magnitude of the added stiffness and damping of linear viscoelastic and viscous damper systems depends not only on the damper but also on the interaction of the damper with other members of the frame. The added stiffness provided by a viscous damper-brace component is negligible under conditions of low frequency and a stiff brace, which plays a more important role than damping in reducing the peak displacement response for impulse excitation. Takewaki and Yoshitomi (1998) showed that the support-member stiffness greatly affects the optimal damper placement and the effects in structural response reduction, and accordingly, should be taken into account in the design of magnitude and placement of the added dampers. Singh et al. (2003) observed that the stiffer the bracing in which a viscous damper is installed, the higher the damper effectiveness in structural response reduction, and suggested that a brace with five times the story stiffness of the structure will be adequate without significantly compromising the damping effectiveness. Chen and Chai (2011) also observed that brace stiffness need not be large in order to achieve a significant level of response reduction for multi-story shear-type buildings with Maxwell model-based brace-damper systems, and concluded that a brace stiffness equal to the first-story stiffness of a structure would be adequate for the desirable levels of response reduction in applications without constraint on the total amount of supplemental damping. Lin and Chopra (2003) found the dependence of structural response reduction on the bracing stiffness varies with the spectral regions of the pseudo-velocity response spectrum of ground motions for structures with nonlinear dampers. Overall, the above research recognized the importance of brace stiffness on damping efficiency and structural performance of viscoelastic and linear viscous damped structures, and recommended using a pragmatic value of brace stiffness in design for compensating for the associated effects of brace flexibility. However, it remains unclear on how the brace stiffness influences the effectiveness of nonlinear viscous dampers and the how the effects of a flexible brace should be taken into account to produce an integrated design of the damping system with the SFRS of structures.

In the experimental study of the response of three-story steel frame structures damped with large-scale nonlinear viscous dampers subjected to the Design basis earthquake (DBE) and the Maximum considered earthquake (MCE) ground motions by Dong et al. (2016, 2018) it was observed that the elastic flexibility in the damper force path of a steel frame building structure along with the nonlinearity of a nonlinear viscous damper causes the viscous damper forces to be partially in phase with the story drifts. This can result in a significant contribution of damper forces to the total story shear force of the structure at times of peak story drifts. As a result, this adds dynamic stiffness to the structure and reduces structural response under transit ground motion excitations. Essentially, this in-phase damper force behavior of nonlinear viscous dampers interacting with structural members should be considered in the seismic design of such structures. Based on these observations, this paper focuses on an in-depth study of the damper force–deformation hysteretic response, effects of brace stiffness, and modeling and equivalent linearization of damper-bracing for seismic design for structural systems with large-scale nonlinear viscous dampers.



2 Characterization of large-scale nonlinear viscous dampers

Large-scale nonlinear viscous dampers with a nominal force capacity of 600 kN and a stroke of \pm 125 mm were used in the characterization tests. The operating ambient temperature range of the dampers is - 7 to + 55 °C. Characterization tests were conducted at the Network for earthquake engineering simulation (NEES) Real time multi directional (RTMD) earthquake simulation facility at Lehigh University (Lehigh RTMD Facility 2014). The characterization test setup is shown schematically in Fig. 2. The actuator is connected to the damper endplate through a short "rigid" transfer beam which is used to adapt to the spacing of the anchors in the strong floor. The actuator and "rigid" transfer beam are supported vertically by rollers that align the actuator with the damper. The damper is connected to a stiff foundation beam using a clevis connection, and the foundation beam is attached to the laboratory strong floor with details that prevent movement between the foundation beam and the strong floor. Tests were conducted at room temperature that varied between 20 and 25°C.

The instrumentation layout of the characterization tests is shown in Fig. 3. A load cell with a capacity of 667 kN is mounted between the damper and the "rigid" transfer beam to measure the damper force. Linear variable displacement transducers (LVDTs) were used to measure the damper deformation and the slip and deformation of the clevis; LVDT-1 and LVDT-2 measure the displacement of the damper endplate relative to the strong floor, referred to as Δ_1 and Δ_2 ; LVDT-3 and LVDT-4 measure the relative displacement between the clevis and the strong floor, referred to as Δ_3 and Δ_4 ; LVDT-5 measures the displacement of damper clevis plate relative to the strong floor, referred to as Δ_5 . The displacements measured by the LVDTs enable two types of damper deformation to be determined, namely damper body deformation u_{bd} and overall damper deformation u_d . u_{bd} is defined as the deformation of the damper body, from the damper endplate to the damper clevis plate, which excludes slip and other deformation in the damper clevis connection. u_{bd} is determined using Eq. (2). u_d is defined as the deformation from the damper endplate to the clevis plates which are welded to the foundation beam. u_d includes slip and other deformation of the clevis connection, such as the deformation of the clevis pin. u_d is determined using Eq. (3). Correspondingly,

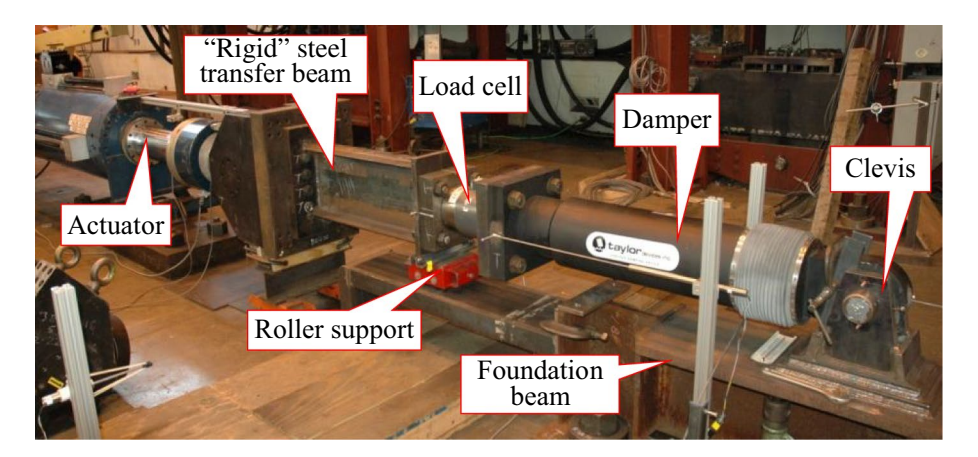


Fig. 2 Test setup for damper characterization tests



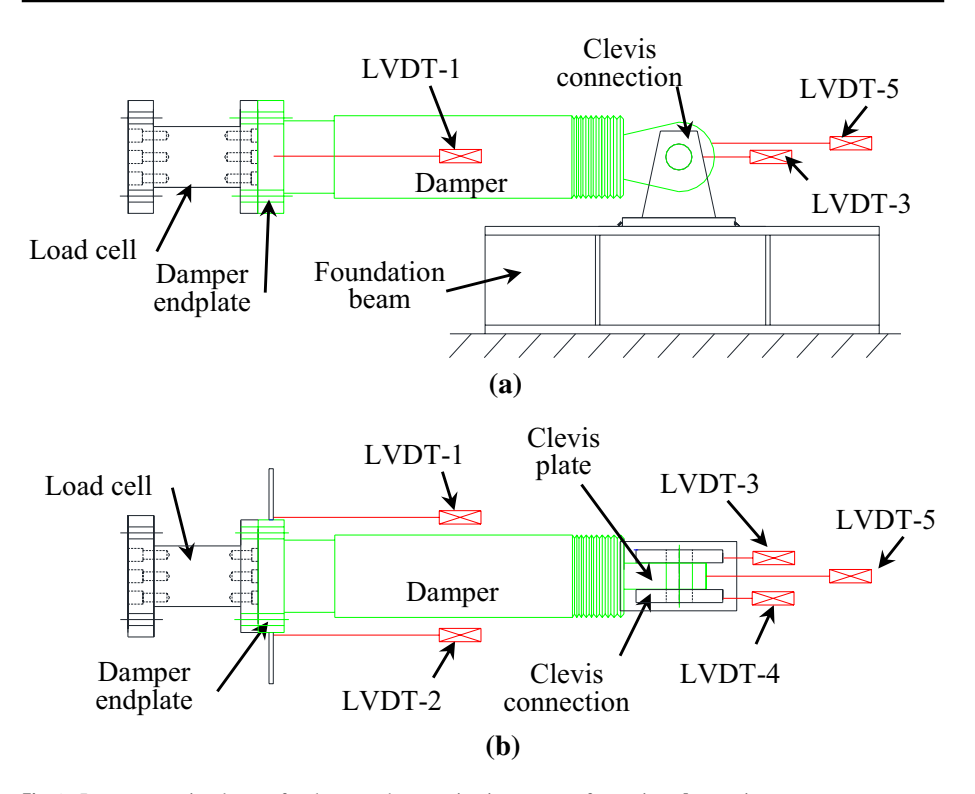


Fig. 3 Instrumentation layout for damper characterization tests: a front view; b top view

the damper body relative velocity $v_{\rm bd}$ and the overall damper relative velocity $v_{\rm d}$ are determined by the finite difference method applied to $u_{\rm bd}$ and $u_{\rm d}$, respectively. $u_{\rm bd}$ and $u_{\rm d}$ are calculated from the measured displacements data as follows:

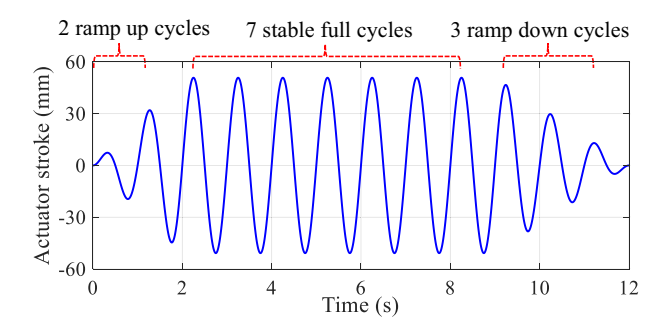
$$u_{\rm bd} = \frac{\Delta_1 + \Delta_2}{2} - \Delta_5 \tag{2}$$

$$u_{\rm d} = \frac{\Delta_1 + \Delta_2}{2} - \frac{\Delta_3 + \Delta_4}{2} \tag{3}$$

The characterization tests used a predefined sinusoidal actuator stroke history shown by example in Fig. 4. The loading history has a total of 12 sinusoidal cycles, including 2 ramp up cycles, 7 full cycles, and 3 ramp down cycles. Considering dampers within a building structure are loaded at amplitudes and frequencies that depend on both the dynamic properties of the structure and the characteristics of earthquake ground motions applied to the structure, a wide range of actuator stroke amplitudes (12.7–101.6 mm) and frequencies (0.25–4.0 Hz) were used in the characterization tests to understand their influence on the response of the nonlinear viscous dampers.



Fig. 4 Typical actuator stroke loading history for damper characterization tests



3 Damper force-deformation response

The damper force-deformation response and damper force-velocity response from the characterization tests are compared based on two types of damper deformation $u_{\rm bd}$ and $u_{\rm d}$ and the associated damper velocity $v_{\rm bd}$ and $v_{\rm d}$. Figure 5 shows the $f_{\rm d}-u_{\rm bd}$ and $f_{\rm d}-v_{\rm bd}$ response, and Fig. 6 shows the $f_{\rm d}-u_{\rm d}$ and $f_{\rm d}-v_{\rm d}$ response under harmonic loading at various frequencies with actuator stroke amplitude of 50.8 mm. In these figures, $f_{\rm d}$ is the measured damper force from the tests. As can be seen, the shape of $f_{\rm d}-u_{\rm bd}$ hysteresis

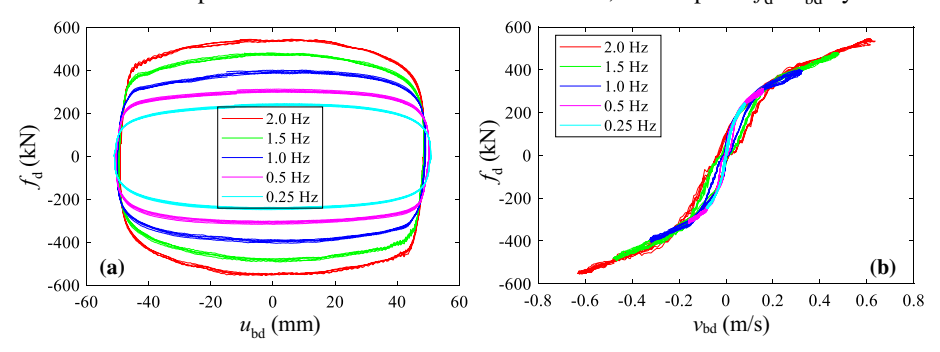


Fig. 5 $f_{\rm d}$ - $u_{\rm bd}$ and $f_{\rm d}$ - $v_{\rm bd}$ hysteretic response of damper under actuator stroke with various frequencies at amplitude of 50.8 mm: $\mathbf{a} f_{\rm d}$ - $u_{\rm bd}$; $\mathbf{b} f_{\rm d}$ - $v_{\rm bd}$

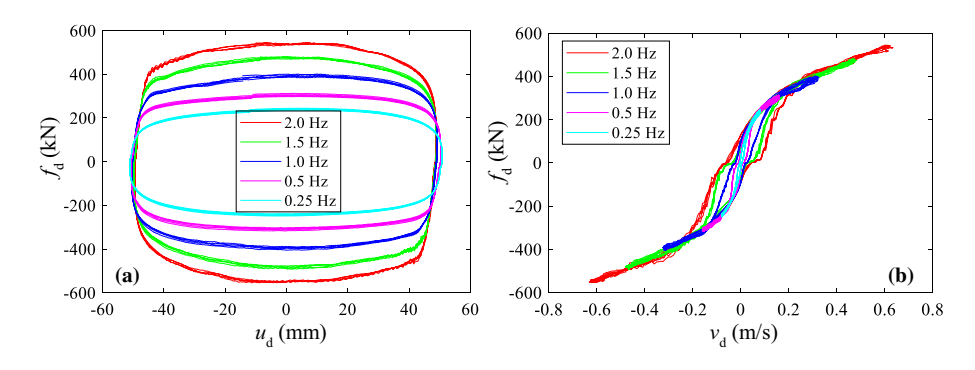


Fig. 6 $f_{d^-}u_d$ and $f_{d^-}v_d$ hysteretic response of damper under actuator stroke with various frequencies at amplitude of 50.8 mm: $\mathbf{a} f_{d^-}u_d$; $\mathbf{b} f_{d^-}v_d$



loop at a lower frequency is more elliptical than that at a higher frequency, which demonstrates the force response of a nonlinear viscous damper depends on loading frequency for a fixed deformation amplitude. Figure 5 indicates the damper force-deformation response of large-scale nonlinear viscous dampers is not purely viscous in two ways: (1) the f_d - u_{bd} hysteresis loops are slightly inclined (i.e., f_d goes toward zero near the peak values of u_{bd} with a slope) in comparison to the theoretical hysteresis loops of a purely viscous damper shown in Fig. 1; and (2) the $f_d - v_{bd}$ response contains a hysteresis loop (i.e., the f_d - v_{bd} response is "inflated" when the relative velocity v_{bd} is near zero) in contrast to the theoretical force-velocity response of a purely viscous damper shown in Fig. 1. The inflation of the f_d - v_{bd} response is most clear in the region when v_{bd} is small, where $f_{\rm d}$ is not zero when $v_{\rm bd}$ is zero and the slope of $f_{\rm d}$ - $v_{\rm bd}$ curves are steeper for unloading than loading. A small jump in v_{bd} is observed when f_d goes to zero, which is related to minor slips within the damper body. The jump is more noticeable in the f_d - v_d response shown in Fig. 6 due to considerable slips in the damper clevis connection. This observed damper response can be explained by the elastic flexibility effect of the damper body (e.g., components including damper cylinder, damper piston, damper endplate and clevis plate). The elastic flexibility effect is more visible when damper force reverses its direction from unloading to reverse loading and diminishes when damper force is near the force peak.

Figure 7a compares the $f_{\rm d}-u_{\rm d}$ response with the $f_{\rm d}-u_{\rm bd}$ response in the same plot, and Fig. 7b compares the $f_{\rm d}-v_{\rm d}$ response with the $f_{\rm d}-v_{\rm bd}$ response in the same plot. It is seen that the $f_{\rm d}-u_{\rm d}$ hysteresis loops are slightly more inclined than the $f_{\rm d}-u_{\rm bd}$ hysteresis loops, and the $f_{\rm d}-v_{\rm d}$ response has more inflation than the $f_{\rm d}-v_{\rm bd}$ response. Compared to $u_{\rm bd}$, the deformation of the clevis connection and slips in the connection are included in $u_{\rm d}$, which increases the elastic flexibility of the damping device and affects damper force–deformation response. The overall slip in $u_{\rm d}$ is 4.0 mm, which leads to a velocity jump up to 0.02 m/s in $v_{\rm d}$ for loading frequency up to 2.0 Hz. As the clevis connection is a part of the damping device to be installed in a structure, it is preferable to use the $f_{\rm d}-u_{\rm d}$ and $f_{\rm d}-v_{\rm d}$ response for the large-scale nonlinear viscous dampers.

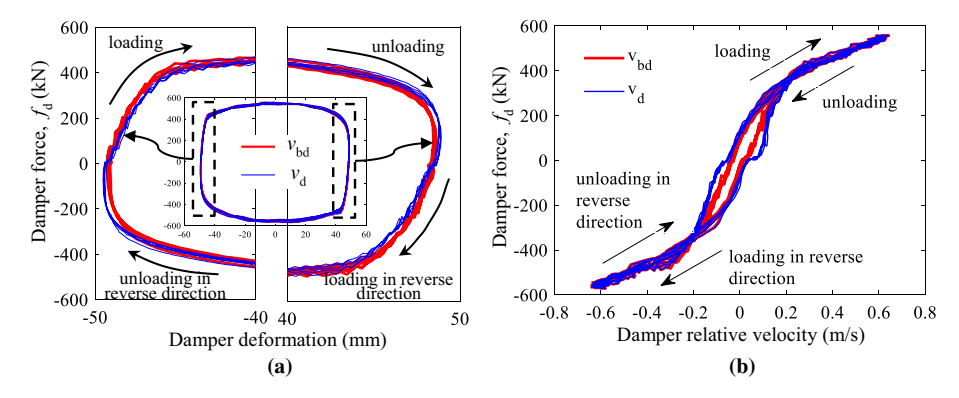


Fig. 7 Comparison of hysteretic response of damper under actuator stroke with frequencies of 2.0 Hz and amplitude of 50.8 mm: a damper force–deformation; b damper force-relative velocity



4 Nonlinear Maxwell model

Based on the damper force–deformation response observed from the characterization tests, a *nonlinear Maxwell* model, shown schematically in Fig. 8a, is proposed for modeling the force–deformation response of large-scale nonlinear viscous dampers. This *nonlinear Maxwell* model comprises of a nonlinear elastic spring and a nonlinear dashpot which are connected in series. The nonlinear elastic spring simulates the nonlinear elastic flexibility in the damper body (e.g., components including damper cylinder, damper piston, damper endplate and clevis plate). Illustrated in Fig. 8b, the nonlinear elastic spring has a stiffness k_{s1} when relative velocity is less than v_{d1} , a stiffness k_{s2} which is greater than k_{s1} when relative velocity is greater than v_{d2} , and a stiffness k_{s} which linearly varies between k_{s1} and k_{s2} over v_{d1} and v_{d2} . The nonlinear dashpot, which simulates the nonlinear viscous behavior of the damper, has a damping coefficient C_{α} and velocity exponent α , as shown in Fig. 8c. The parameters C_{α} , α , k_{s1} , k_{s2} , v_{d1} , and v_{d2} of the model were identified using the force–deformation and force–velocity response from the characterization tests.

As the nonlinear elastic spring and nonlinear dashpot are connected in series in the *nonlinear Maxwell* model, the force of the model equals to the force in the spring and the dashpot as expressed in Eq. (4), and the total deformation and relative velocity of the model are the sums of the deformations and relative velocities in the spring and dashpot, as expressed in Eq. (5) and Eq. (6), respectively.

$$f_{\rm d} = f_{\rm s} = f_{\rm c} \tag{4}$$

$$u_{\rm d} = u_{\rm s} + u_{\rm c} \tag{5}$$

$$v_{\rm d} = v_{\rm s} + v_{\rm c} \tag{6}$$

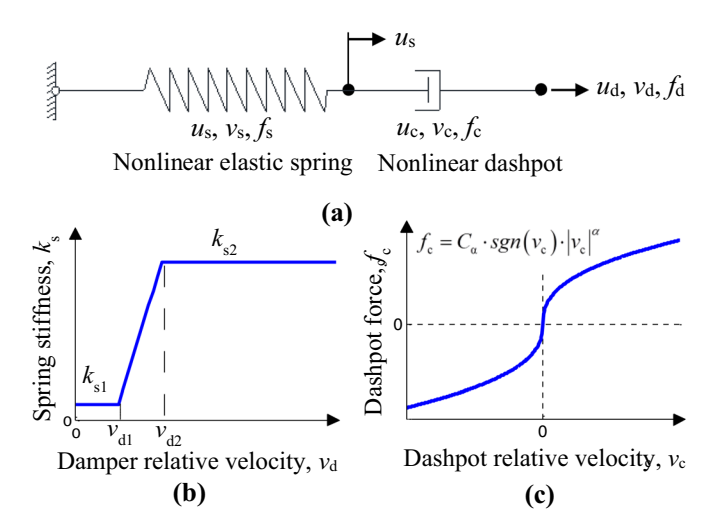


Fig. 8 Nonlinear Maxwell damper model: $\bf a$ schematic of model; $\bf b$ nonlinear elastic spring model; $\bf c$ nonlinear dashpot model



where $f_{\rm d}f_{\rm c}$, and $f_{\rm s}$ are the damper force, dashpot force, and spring force, respectively; $u_{\rm d},u_{\rm c}$, and $u_{\rm s}$ are the total damper deformation, dashpot deformation, and spring deformation, respectively; and $v_{\rm d},v_{\rm c}$, and $v_{\rm s}$ are the total damper relative velocity, dashpot relative velocity, and spring relative velocity, respectively. The dashpot force and the spring force can be expressed as:

$$f_{\rm s} = k_{\rm s} \cdot u_{\rm s} \tag{7}$$

$$f_{c} = C_{\alpha} \cdot sgn(v_{c}) \cdot |v_{c}|^{\alpha}$$
(8)

Accordingly, Eq. (5) and Eq. (6) can be written as:

$$u_{\rm d} = \frac{C_{\alpha} \cdot sgn(v_{\rm c}) \cdot |v_{\rm c}|^{\alpha}}{k_{\rm c}} + u_{\rm c} \tag{9}$$

$$v_{\rm d} = \frac{1}{k_{\rm s}} \frac{\delta f_{\rm d}}{\delta t} + v_{\rm c} \tag{10}$$

Equation (9) indicates that when $k_s \to \infty$, $u_d \approx u_c$. For k_s with a finite stiffness, when $v_c > 0$, u_c is increasing but smaller than u_d ; and when $v_c < 0$, u_c is decreasing but greater than u_d . Therefore, the dashpot relative velocity is not zero when at the peak damper deformation u_d , which leads to nonzero dashpot force and damper force. This model behavior explains the inclination of the $f_d - u_d$ hysteresis loops of the characterized nonlinear viscous dampers near the peak values of u_{bd} and u_d , where the rate of damper force decreases toward zero (i.e., unloading) is more rapid than the rate of damper fore increases from zero (i.e., loading).

Equation (10) indicates that when $k_s \to \infty$, $v_d \approx v_c$, which suggests that the $f_d - v_d$ hysteresis loops of the damper is equivalent to that of a nonlinear viscous dashpot. For k_s with a finite stiffness, v_d is smaller than v_c when f_d is decreasing (i.e., $\frac{\delta f_d}{\delta t} < 0$), and v_d is greater than v_c when f_d is increasing (i.e., $\frac{\delta f_d}{\delta t} > 0$). This model behavior explains the inflation of the $f_d - v_d$ hysteresis loops in Fig. 6, where the slope of the hysteresis loops are steeper for unloading than loading near zero velocity region.

The nonlinear elastic spring in the *nonlinear Maxwell* model accounts for the effect of varied spring stiffness over damper relative velocity. To demonstrate this effect,

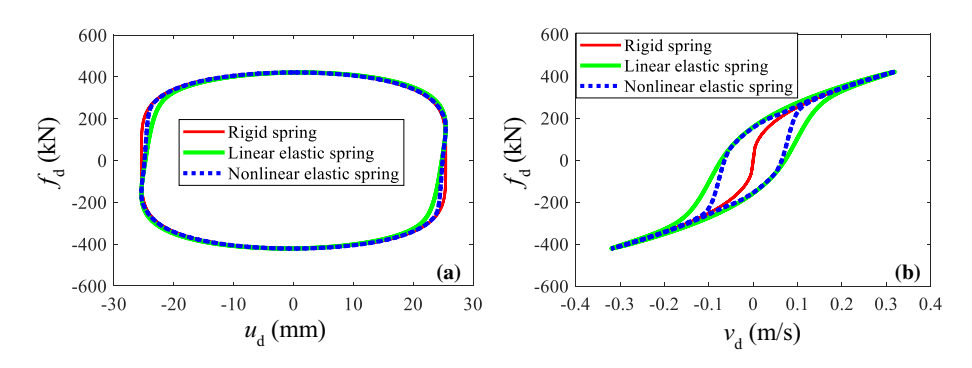


Fig. 9 Effect of nonlinear elastic spring on damper response: $\mathbf{a} f_d - u_d$; $\mathbf{b} f_d - v_d$

Fig. 9 shows the comparison of hysteretic response of damper models with rigid spring, linear elastic spring, and nonlinear elastic spring, respectively. The linear elastic spring has a constant stiffness $k_{\rm s}=175\times10^3$ kN/m, while the nonlinear elastic spring has $k_{\rm s1}=175\times10^3$ kN/m, $k_{\rm s2}=10k_{\rm s1}$, $v_{\rm d1}=0.05$ m/s, and $v_{\rm d2}=0.20$ m/s. It can be seen that, unlike the model with rigid spring, the hysteretic response of the model with linear and nonlinear springs have inclination in the $f_{\rm d}-u_{\rm d}$ hysteresis loops and inflation in the $f_{\rm d}-v_{\rm d}$ hysteresis loops. Compared to the model with linear elastic spring, the model with the nonlinear elastic spring better captures the inclination in the $f_{\rm d}-u_{\rm d}$ hysteresis loops and inflation in the $f_{\rm d}-v_{\rm d}$ hysteresis loops.

The damping coefficient C_{α} and velocity exponent α can be identified using test data with $f_{\rm d}$ measured from characterization tests and $v_{\rm bd}$ derived by finite difference of $u_{\rm bd}$. The theoretical damper force-velocity relationship for a viscous damper in the form of Eq. (1) was used to identify C_{α} and α by curve fitting the test data using the least-squares method. The data with f_d at pick v_{bd} in each characterization test was used for the identification. This identification of C_{α} and α using Eq. (1) essentially neglects the effect of elastic flexibility on damper response when damper force is large, which is valid based on two facts: (i) the elastic flexibility effect diminishes with the increase of damper force as observed from the characterization tests; (ii) the spring deformation and damper deformation (i.e., u_s and u_d) of the model are at their minimums when damper force is large. The values of $C_{\alpha} = 696 \text{ kN} - (\text{s/m})^{0.44}$ and $\alpha = 0.44$ were identified for the dampers. Subsequently, the values of k_{s1} , k_{s2} , v_{d1} , and v_{d2} were identified by minimizing the discrepancy between the response predicted by the model and the response measured from the characterization tests. The identified parameters are $k_{\rm s1} = 219 \times 10^3$ kN/m, $k_{s2} = 10k_{s1}$, $v_{d1} = 0.07$ m/s, and $v_{d2} = 0.21$ m/s. Figure 10 compares the damper hysteretic response predicted by the nonlinear Maxwell model with the identified parameters with that measured from the characterization tests. Hysteretic responses of the complete five loops that begin with the third loop and end with the eighth loop under the full sinusoidal cycle of actuator stroke loading history are plotted in the figure for comparison. As shown, the nonlinear Maxwell model overall predicts accurate damper force-deformation response with inclusions of the inclination of the f_d - u_d hysteresis loops and the inflation of the f_d - v_d hysteresis loops.

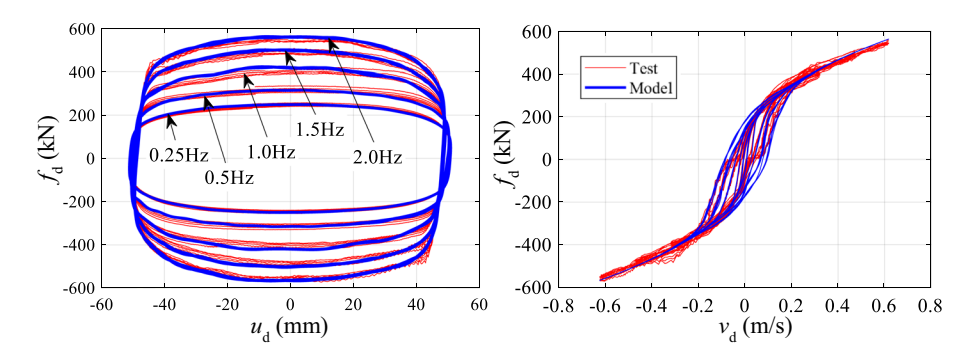


Fig. 10 Comparison of damper response from test and damper model prediction at actuator stroke amplitude of 50.8 mm



5 Equivalent linearization of damper response

5.1 Equivalent linear elastic-viscous model for damper-brace component

The equivalent linearization of nonlinear viscous damper response aims to include the two primary features of the damper response in structural response prediction for seismic design, i.e., (i) damper nonlinearity, and (ii) damper interaction with the elastic structural components in the complete damper force path. Demonstrated by results from the real-time hybrid earthquake simulations (Dong et al. 2016), the elastic flexibility of the structural components in the complete damper force path have notable effects on structural response, which should be considered in the seismic design of structures with large-scale nonlinear viscous dampers. The equivalent linearization of the nonlinear viscous damper force—deformation response is enabled using an equivalent elastic-viscous model. Fan (1998) and Lee et al. (2005) used the equivalent elastic-viscous model for analysis of reinforced concrete frame with viscoelastic dampers. To model a Single degree-of-freedom (SDOF) system damped with a viscoelastic damper, the equivalent elastic-viscous model contains a spring to model the equivalent elastic stiffness of the system and a dashpot to model the equivalent viscous damping based on the concept of equivalent energy dissipation for the SDOF system.

Figure 11a shows a SDOF system, representing a one-story frame structure equipped with a nonlinear viscous damper. The SDOF system includes the floor mass m, the initial stiffness of the structure without the damper k_0 , and the brace stiffness in the horizontal direction k_b . The brace stiffness represents the elastic flexibility of all the structural components which connect the damper to the floor mass of the structure, i.e., k_b represents all the elastic flexibility in the damper force path. The nonlinear viscous damper has damping coefficient C_α and velocity exponent α . This system can be idealized as an SDOF model as shown in Fig. 11b. In this model, the frame structure without damper is represented by the elastic Spring-1, and the damper-brace component (i.e., the nonlinear viscous damper and associated brace) is represented by the *nonlinear Maxwell* damper model which consists of the elastic Spring-2 for the brace and the nonlinear dashpot for the nonlinear viscous damper in series.

In the time domain, the relationship between story drift u(t), damper deformation $u_{\rm d}(t)$, and brace deformation $u_{\rm b}(t)$ for the damper-brace component shown in Fig. 12a can be expressed as:

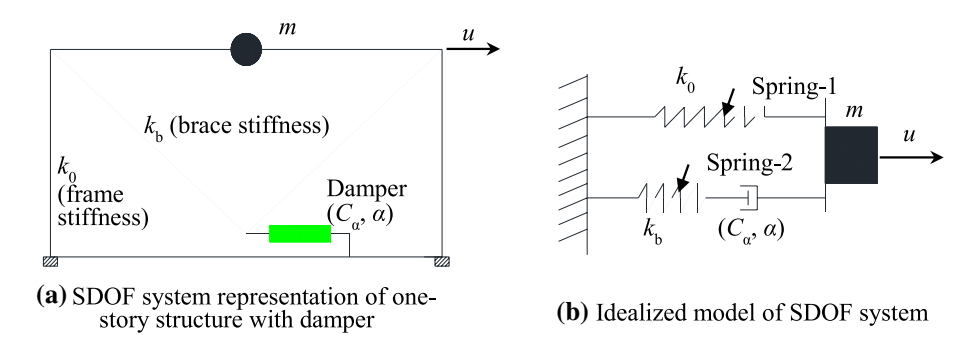


Fig. 11 SDOF analytical model of one-story structure with nonlinear viscous damper

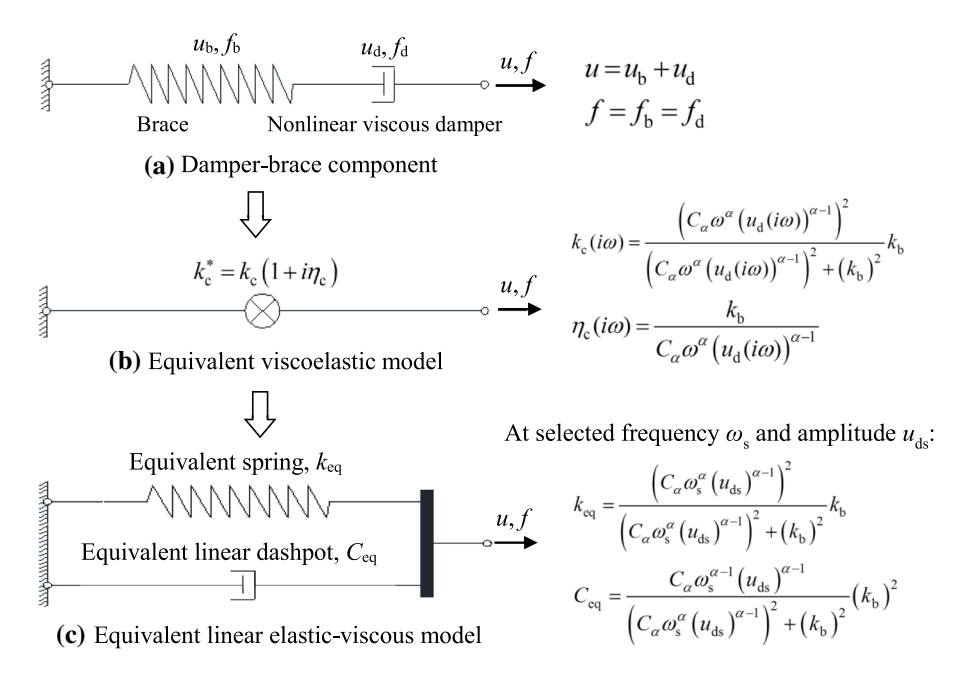


Fig. 12 Equivalent linear elastic-viscous model for damper-brace component

$$u(t) = u_{\mathsf{b}}(t) + u_{\mathsf{d}}(t) \tag{11}$$

In the frequency domain, the damper velocity can be expressed as the derivative of damper deformation as follows:

$$\dot{u}_{\rm d}(i\omega) = i\omega \cdot u_{\rm d}(i\omega) \tag{12}$$

where $u_d(i\omega)$ is the Fourier transform of the damper deformation $u_d(t)$ and i is the imaginary unit of frequency ω . The damper force in the frequency domain can be expressed as:

$$f_{\rm d}(i\omega) = iC_{\alpha}\omega^{\alpha} \cdot \left(u_{\rm d}(i\omega)\right)^{\alpha} \tag{13}$$

Let,

$$k_{\rm d}(i\omega) = iC_{\alpha}\omega^{\alpha} \cdot \left(u_{\rm d}(i\omega)\right)^{\alpha - 1} \tag{14}$$

Then,

$$f_{\rm d}(i\omega) = k_{\rm d}(i\omega) \cdot u_{\rm d}(i\omega)$$
 (15)

where $k_{\rm d}(i\omega)$ is the dynamic stiffness of the damper that varies with loading frequency ω and damper deformation $u_{\rm d}(i\omega)$.

The combined stiffness for the damper-brace component is as follows:



$$k_{\mathrm{c}}^{*}(i\omega) = \frac{1}{\frac{1}{k_{\mathrm{b}}} + \frac{1}{k_{\mathrm{d}}(i\omega)}} = \frac{\left(C_{\alpha}\omega^{\alpha}\left(u_{\mathrm{d}}(i\omega)\right)^{\alpha-1}\right)^{2}}{\left(C_{\alpha}\omega^{\alpha}\left(u_{\mathrm{d}}(i\omega)\right)^{\alpha-1}\right)^{2} + \left(k_{\mathrm{b}}\right)^{2}} k_{\mathrm{b}} + i \frac{C_{\alpha}\omega^{\alpha}\left(u_{\mathrm{d}}(i\omega)\right)^{\alpha-1}}{\left(C_{\alpha}\omega^{\alpha}\left(u_{\mathrm{d}}(i\omega)\right)^{\alpha-1}\right)^{2} + \left(k_{\mathrm{b}}\right)^{2}} (k_{\mathrm{b}})^{2}$$

$$(16)$$

 $k_{\rm c}^*(i\omega)$ is the complex stiffness for the equivalent viscoelastic model, as shown in Fig. 12(b), which can be expressed as follows:

$$k_{\rm c}^*(i\omega) = k_{\rm c}(i\omega) (1 + i\eta_{\rm c}(i\omega))$$
 (17a)

$$k_{c}(i\omega) = \frac{\left(C_{\alpha}\omega^{\alpha}\left(u_{d}(i\omega)\right)^{\alpha-1}\right)^{2}}{\left(C_{\alpha}\omega^{\alpha}\left(u_{d}(i\omega)\right)^{\alpha-1}\right)^{2} + \left(k_{b}\right)^{2}}k_{b}$$
(17b)

$$\eta_{\rm c}(i\omega) = \frac{k_{\rm b}}{C_{\alpha}\omega^{\alpha} (u_{\rm d}(i\omega))^{\alpha-1}}$$
(17c)

 $k_{\rm c}(i\omega)$ and $\eta_{\rm c}(i\omega)$ are the storage stiffness and loss factor of the equivalent viscoelastic model, which are dependent on the brace stiffness and the frequency and amplitude of damper deformation. For rigid brace $(k_{\rm b} \to \infty)$, $k_{\rm c}(i\omega)$ would approach zero and $\eta_{\rm c}(i\omega)$ would approach infinity, so that the equivalent viscoelastic model for the damper-brace component would not have an elastic storage stiffness and would have an infinitely large loss factor. For a linear viscous damper with $\alpha=1$, $k_{\rm c}(i\omega)$ and $\eta_{\rm c}(i\omega)$ become:

$$k_{c1}(i\omega) = \frac{(C_1\omega)^2}{(C_1\omega)^2 + (k_b)^2} k_b$$
 (18a)

$$\eta_{c1}(i\omega) = \frac{k_b}{C_1\omega} \tag{18b}$$

For a given C_1 , $k_{c1}(i\omega)$ and $\eta_{c1}(i\omega)$ are only dependent on the frequency and brace stiffness.

The equivalent linear elastic-viscous model, as shown in Fig. 12c, includes a linear elastic spring and a linear dashpot. The stiffness of the linear elastic spring $k_{\rm eq}$ and the viscous damping coefficient of the linear dashpot $C_{\rm eq}$ can be determined for a selected frequency $\omega_{\rm s}$, and a selected damper deformation amplitude $u_{\rm ds}$. In practice, $\omega_{\rm s}$ can be selected as the natural frequency of a structure, and $u_{\rm ds}$ can be estimated from the maximum story drift u_0 which can be estimated as the design story drift limit. With selected $\omega_{\rm s}$ and $u_{\rm ds}$, the dynamic stiffness of the damper $k_{\rm d}$ can be determined as $k_{\rm d} = C_a \omega_{\rm s}^{\alpha} \cdot \left(u_{\rm ds}\right)^{\alpha-1}$. Since the damper deformation is not equal to the story drift as usual, iteration is required to determine $u_{\rm ds}$ from u_0 based on the stiffness ratio $k_{\rm b}/k_{\rm d}$, i.e., $u_{\rm ds} = k_{\rm b}/\left(k_{\rm b} + k_{\rm d}\right) \cdot u_0$. The equivalent stiffness $k_{\rm eq}$ equals $k_{\rm c}$ (i.e., the real part of the combined complex stiffness $k_{\rm c}^*$) evaluated at $\omega_{\rm s}$ and $u_{\rm ds}$, as Eq. (19). By equating the energy dissipation per harmonic cycle of the damper-brace component to the energy dissipation per harmonic cycle of the equivalent linear elastic-viscous model, $C_{\rm eq}$ is obtained as Eq. (20).



$$k_{\text{eq}} = k_{\text{c}}(i\omega_{\text{s}}) = \frac{\left(C_{\alpha}\omega_{\text{s}}^{\alpha}\left(u_{\text{ds}}\right)^{\alpha-1}\right)^{2}}{\left(C_{\alpha}\omega_{\text{s}}^{\alpha}\left(u_{\text{ds}}\right)^{\alpha-1}\right)^{2} + \left(k_{\text{b}}\right)^{2}}k_{\text{b}}$$

$$(19)$$

$$C_{\text{eq}} = \frac{k_{\text{c}}(i\omega_{\text{s}})\eta_{\text{c}}(i\omega_{\text{s}})}{\omega_{\text{s}}} = \frac{C_{\alpha}\omega_{\text{s}}^{\alpha-1}(u_{\text{ds}})^{\alpha-1}}{\left(C_{\alpha}\omega_{\text{s}}^{\alpha}(u_{\text{ds}})^{\alpha-1}\right)^{2} + \left(k_{\text{b}}\right)^{2}} (k_{\text{b}})^{2}$$
(20)

Similar to the stiffness $K_{\rm damper}$ due to the in-phase behavior of damper force with story drift, which adds story stiffness to the structure, as observed from the experimental results by Dong et al. (2016), $k_{\rm eq}$ adds stiffness to the SDOF system. As a result, the equivalent model for the SDOF system, shown in Fig. 11, has an effective stiffness $k_{\rm eff}$ and effective equivalent damping ratio $\xi_{\rm eff}$ as follows:

$$k_{\text{eff}} = k_0 + k_{\text{eq}} = k_0 + \frac{\left(C_\alpha \omega_s^\alpha (u_{\text{ds}})^{\alpha - 1}\right)^2}{\left(C_\alpha \omega_s^\alpha (u_{\text{ds}})^{\alpha - 1}\right)^2 + \left(k_{\text{b}}\right)^2} k_{\text{b}}$$
(21)

$$\xi_{\text{eff}} = \frac{C_{\text{eq}}}{2m\omega_{\text{eff}}} = \frac{\eta_{\text{c}}}{2} \frac{k_{\text{eq}}}{k_{\text{eff}}} \frac{\omega_{\text{eff}}}{\omega_{\text{s}}}$$
(22)

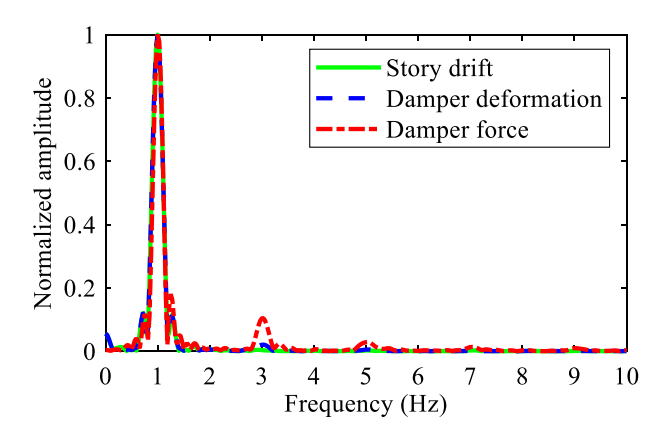
where $\omega_{\text{eff}} = \sqrt{k_{\text{eff}}/m}$ is the natural frequency of the SDOF system with the damper.

The equivalent linearization of the damper response using the equivalent linear elastic-viscous model has an underlying assumption that the damper force output from this model has the same frequency content as the damper deformation input. This assumption is made when going from Eq. (13), where the damper force and damper deformation are expressed as functions of a continuous frequency variable ω , to Eq. (19) and Eq. (20), where the equivalent properties (i.e., $k_{\rm eq}$ and $C_{\rm eq}$) are expressed as functions of a single frequency $\omega_{\rm s}$, even though an applied damper deformation at a single frequency will produce force output at multiple frequencies. The assumption of single frequency response is not strictly true due to the nonlinearity of the damper-brace component, however, makes sense for the equivalent linearization of the nonlinear viscous damper force—deformation response using the equivalent linear elastic-viscous model, as the dominant component of the damper response is at the frequency of the story drift input, as demonstrated below.

Figure 13 shows the frequency response amplitudes of damper deformation and damper force determined from the *nonlinear Maxwell* model using a predefined harmonic story drift as the input. The predefined harmonic story drift has an amplitude of 12 mm and a frequency of 1.0 Hz. The frequency response amplitude of the predefined story drift is also shown in Fig. 13. The frequency response amplitudes of story drift, damper deformation, and damper force were obtained from the Fast fourier transform (FFT) of the responses. Here, the *nonlinear Maxwell* model represents the damper and associated brace in the damper force path. The damping coefficient $C_{\alpha} = 696 \, \text{kN} \cdot (\text{s/m})^{0.44}$ and velocity exponent $\alpha = 0.44$, and a practical brace flexibility with $k_{\rm b} = 135 \times 10^3 \, \text{kN/m}$ were used in this model. As shown in Fig. 13, the damper force has components at frequencies higher than 1.0 Hz (e.g., 3.0 Hz, 5.0 Hz, 7.0 Hz, etc.), while the first story drift has significant frequency response amplitude at only 1.0 Hz. The damper deformation also has components



Fig. 13 Frequency response of damper deformation and damper force from model prediction with α = 0.44 using predefinded story drift input



at frequencies higher than 1.0 Hz, which is expected because the damper force has components at these higher frequencies. The higher frequencies in the damper deformation can be understood as follows: (1) the damper force components at higher frequencies require that force components at higher frequencies develop in the spring (i.e., the brace) of the damper-brace component to provide force equilibrium; (2) the force components at higher frequencies in the spring require spring deformation components at higher frequencies due to the linear elastic constitutive property of the spring; (3) the spring deformation components at higher frequencies require damper deformation components at higher frequencies so that the sum of the spring and damper deformation is compatible with the harmonic story drift.

The effect of damper nonlinearity on the damper force frequency response can be observed by the comparison between Fig. 13 and Fig. 14, where the frequency response amplitude of the story drift, damper deformation, and damper force from the *nonlinear Maxwell* model with different values for velocity exponent α within the damper-brace component are shown. Figure 14a and Fig. 14b show the frequency response amplitudes of the story drift, damper deformation, and damper force from the model with $\alpha = 0.2$ (more nonlinearity) and $\alpha = 0.8$ (less nonlinearity), respectively. It is seen that the frequency response amplitudes of damper force and damper deformation in Fig. 14a are greater than those in

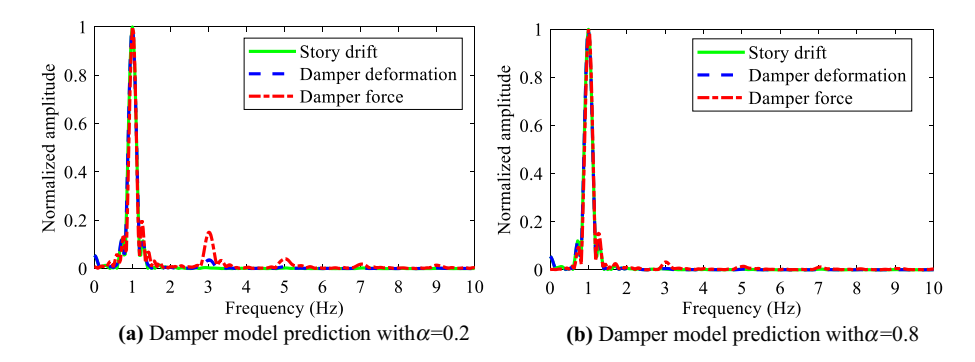


Fig. 14 Frequency response of damper deformation and damper force from model prediction for different damper nonlinearity in damper-brace component

Fig. 13, while the frequency response amplitudes of damper force and damper deformation in Fig. 14b are smaller than those in Fig. 13, which indicates that the frequency response amplitudes of damper force and damper deformation components at higher frequencies increase as the nonlinearity in the damper-brace component increases.

These results show that, although the damper force response has components at higher frequencies and the amplitudes of these components increase with the increase of nonlinearity in the damper-brace component, the dominant component of the damper force response is at the frequency of the story drift input. These results justify the assumption that a single frequency can be used in the equivalent linearization of the nonlinear viscous damper force—deformation response using the equivalent linear elastic-viscous model for α values in the range that was studied.

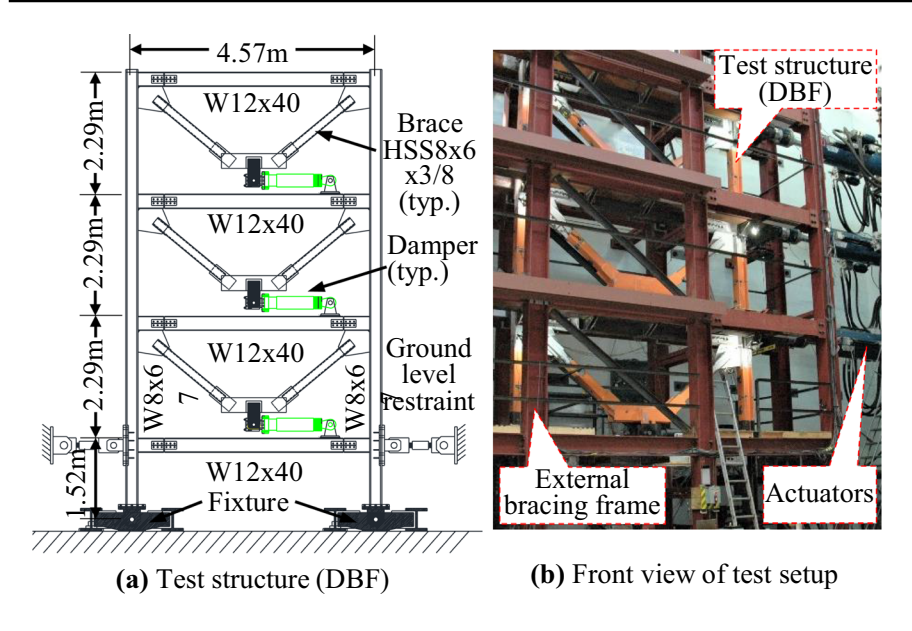
5.2 Validation of equivalent linear elastic-viscous model

The equivalent linear elastic-viscous model is validated using results from harmonic tests on a 0.6-scale three-story structure with one nonlinear viscous damper and the associated brace in each story, see Fig. 15a. The test structure is referred to as the Damped braced frame (DBF). The elevation and plan views of the test structure in the test setup are shown in Fig. 15b, c, respectively. The DBF is laterally braced by an external bracing frame which is fixed to the reaction wall. During the test, loading is applied to the DBF at the loading plates through pretensioned loading beams connected to actuators. The dampers installed in the DBF have damping coefficient $C_{\alpha} = 696 \text{ kN} - (\text{s/m})^{0.44}$ and velocity exponent $\alpha = 0.44$. The complete force path for the damper in each story includes columns, beams, brace, brace extensions, gusset plates, clevises, damper attachment plates, pins, bolts, and other components required to connect the damper to the mass of the floor levels (i.e., seismic mass degrees of freedom) of the structure. The elastic flexibility of each component in the force path contributes the total flexibility of the complete force path for the damper.

During the harmonic tests, the DBF was subjected to predefined harmonic floor displacement histories with frequencies of 1.0 and 2.0 Hz, respectively. The amplitudes of the predefined floor displacements were the same for each test, with values of 12, 24, and 36 mm for the first, second, and third floor, respectively. Figure 16 shows the predefined floor displacement time histories as the input for the actuators. Figure 17 shows the instrumentation for the floor displacement and damper deformation measurements in the DBF. During the tests, temposonic displacement transducers with a range of ±380 mm were used to measure floor displacements. Each temposonic is attached to the external bracing frame and attached to the top flange of the DBF floor beam at midspan, as shown in Fig. 17a. The floor displacement measurements were used to determine the story drifts of the DBF. LVDTs were mounted on each damper between damper clevis and the damper end plate to measure the damper deformation, as shown in Fig. 17b. The damper deformation is defined as the total of the deformation measured by LVDT-1 and LVDT-2. A load cell with a force capacity of ±660 kN was placed in the damper-brace connection to measure the damper force in each story.

For the validation of the equivalent linear elastic-viscous model, the story drifts of the DBF were used as the deformation input (u) to the model for the force output. The story drift amplitudes determined from the floor displacement measurements during the tests with predefined floor displacement histories were fairly uniform over the height of the building and used as the deformation input (u_m) to the equivalent linear elastic-viscous model for the damper-brace component in each story of the DBF. Given u_m





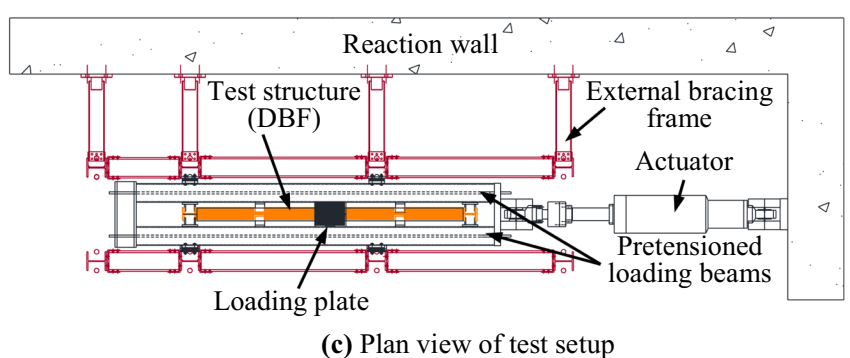


Fig. 15 Test structure with nonlinear viscous dampers

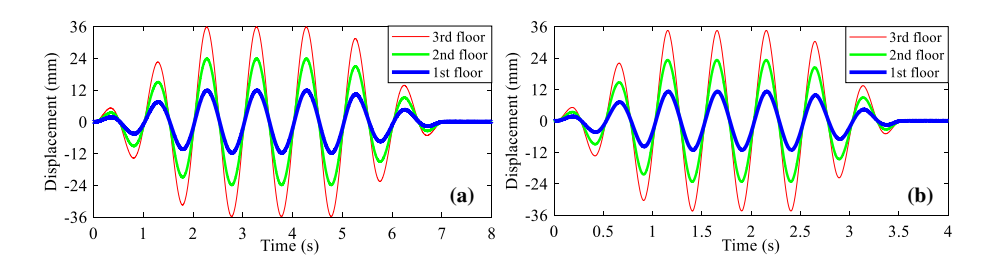


Fig. 16 Predefined floor displacement time histories with frequency of: a 1.0 Hz; b 2.0 Hz

and frequency ω of the loading, the deformation amplitude $u_{\rm ds}$ and dynamic stiffness $k_{\rm d}=C_{\alpha}\omega^{\alpha}\cdot\left(u_{\rm ds}\right)^{\alpha-1}$ of the damper were estimated iteratively, which were used to calculate $k_{\rm eq}$ and $C_{\rm eq}$ for the equivalent linear elastic-viscous model. To demonstrate the



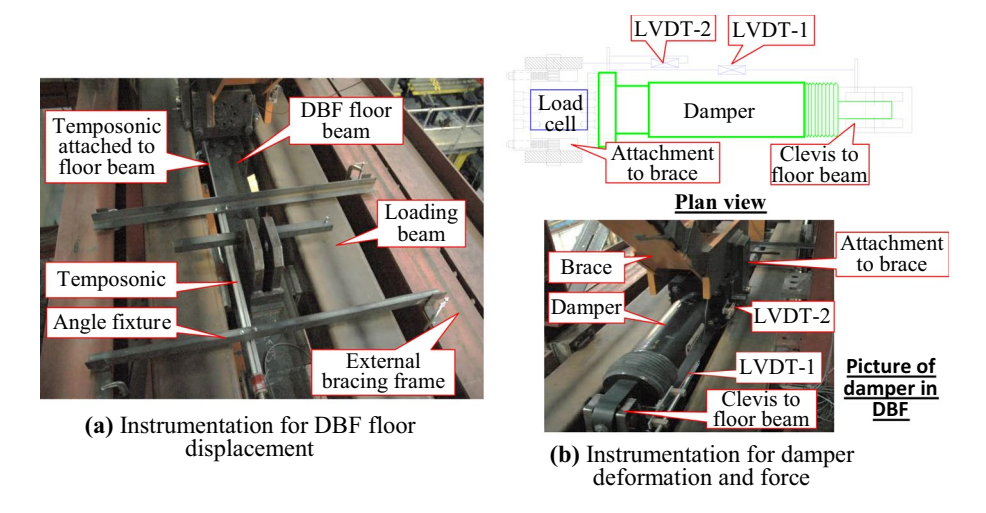


Fig. 17 Instrumentaiton for test structure

accuracy of the equivalent linear elastic-viscous model, the predicted damper forces using the *equivalent linear elastic-viscous model* are compared with the damper forces measured from the harmonic tests, as shown in Fig. 18 for the damper force time histories and Fig. 19 for the damper force-story drift hysteresis loops. In these plots, the story drifts were calculated from the measured floor displacement histories from the harmonic tests. As can be seen, for the loops with story drift amplitudes matching the amplitudes used in the linearization of the model, the damper force-story drift hysteresis loops from the equivalent linear elastic-viscous model agree well with the damper

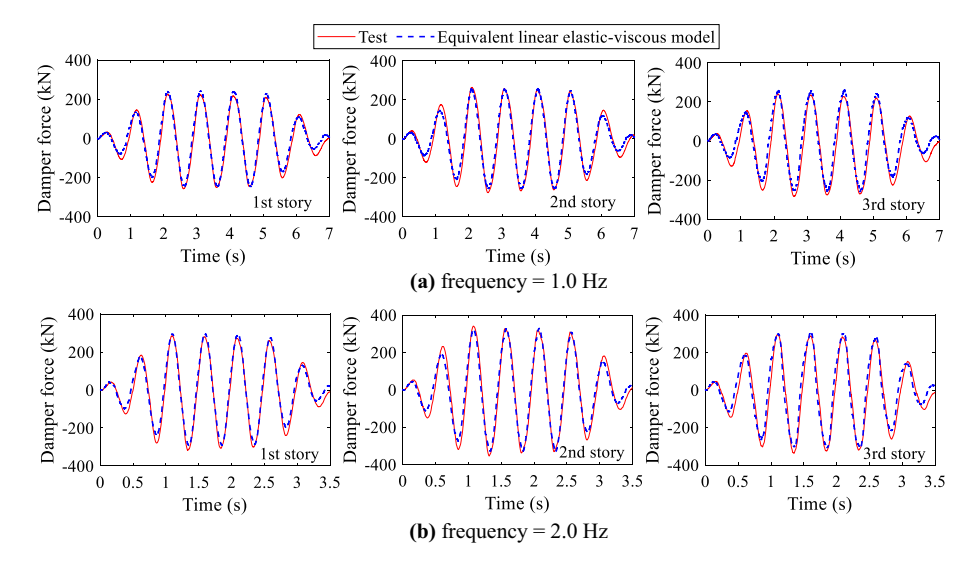


Fig. 18 Comparison of damper force time histories from tests and equivalent linear elastic-viscous model



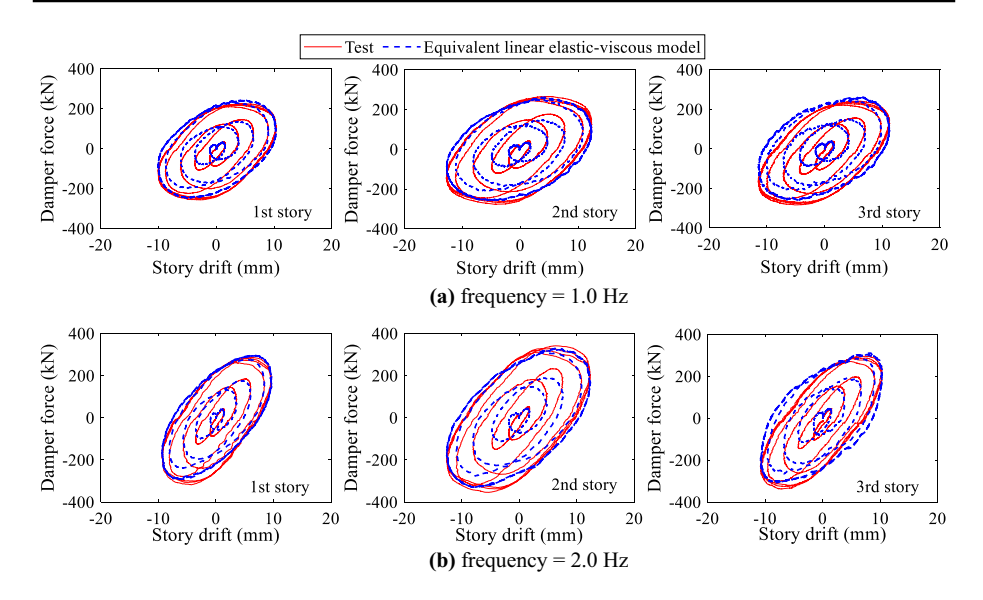


Fig. 19 Comparison of damper force-story drift hysteresis behavior from tests and equivalent linear elastic-viscous model

force-story drift hysteresis loops obtained from the tests, which validates that the equivalent linear elastic-viscous model is suitable for preliminary analysis of a structure with nonlinear viscous dampers.

6 Effects of brace stiffness on effective stiffness and equivalent damping ratio

Using the equivalent linear elastic-viscous model, the effects of elastic flexibility of brace on the effective stiffness and equivalent damping ratio of a 0.6-scaled three-story test structure with a Moment resisting frame (MRF) and a DBF with nonlinear viscous dampers are studied, see Fig. 20a. The MRF represents the Lateral force-resisting system (LFRS) while the DBF represents the supplemental damping energy dissipation system for a prototype office building, see Fig. 20b. The pair of MRF and DBF work in parallel through the action of the floor diaphragm and represents the LFRS and damping system in one horizontal direction of one-quarter of the total floor area of the building. The design philosophy of the prototype building was that the MRFs are designed to satisfy the strength criterion of ASCE 7-16 and the DBFs with dampers are added to achieve design performance objectives, including limiting story drift at prescribed hazard levels in order to control story drift. The design details of the members of the MRF and DBF can be found in Dong (2016). In the test structure, the brace stiffness (k_b) is defined as the combined stiffness of the complete force path for the damper in each story of the DBF, which include the pins, bolts, clevises, gusset plates, braces, brace extensions, and other components required to connect the damper to the seismic mass Degree-of-freedom (DOF) at each floor of the structure. The story stiffness matrix \mathbf{K}_0 and mass matrix \mathbf{M} of the structure without dampers are as:



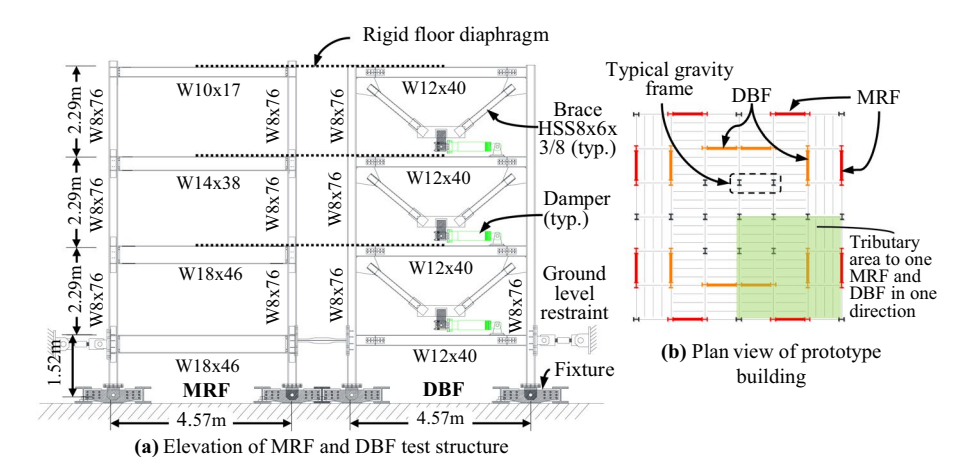


Fig. 20 0.6-scaled test structure with MRF and DBF

$$\mathbf{K}_{0} = \begin{bmatrix} k_{01} + k_{02} & -k_{02} & 0\\ -k_{02} & k_{02} + k_{03} & -k_{03}\\ 0 & -k_{03} & k_{03} \end{bmatrix} = \begin{bmatrix} 63.4 & -23.6 & 0.0\\ -23.6 & 37.2 & -13.6\\ 0.0 & -13.6 & 13.6 \end{bmatrix} \times 10^{3} \,\mathrm{kN/m}$$
 (23)

$$\mathbf{M} = \begin{bmatrix} m_1 & 0 & 0 \\ 0 & m_2 & 0 \\ 0 & 0 & m_3 \end{bmatrix} = \begin{bmatrix} 101.2 & 0.0 & 0.0 \\ 0.0 & 101.2 & 0.0 \\ 0.0 & 0.0 & 73.5 \end{bmatrix} \text{kN} - \text{s}^2/\text{m}$$
 (24)

where k_{01} , k_{02} , and k_{03} is the story stiffness of the first, second, and third story of the test structure including the MRF and DBF without dampers, respectively; m_1 , m_2 , and m_3 is the floor mass of the first, second, and third floor of the structure, respectively. The ratio of brace stiffness k_b per story in the global direction to the first story stiffness k_{01} is expressed as $\alpha_b = k_b/k_{01}$, and the ratio of dynamic stiffness of damper k_d to k_{01} is expressed as $\beta_d = k_d/k_{01}$, where k_d is determined based on ω_s and u_{ds} as $k_d = C_\alpha \omega_s^\alpha \cdot \left(u_{ds}\right)^{\alpha-1}$. And k_{eff}/k_{01} and T_{eff}/T_0 are expressed as follows:

$$k_{\text{eff}}/k_{01} = 1 + \frac{(\beta_{\text{d}})^2}{(\beta_{\text{d}})^2 + (\alpha_{\text{b}})^2} \alpha_{\text{b}}$$
 (25)

$$T_{\text{eff}}/T_0 = \sqrt{\frac{1}{1 + \frac{(\beta_d)^2}{(\beta_d)^2 + (\alpha_b)^2}} \alpha_b}$$
 (26)

Figure 21 shows the trend of $k_{\rm eff}/k_{01}$ over the loading frequency $(\omega/2\pi)$ for varied story drift amplitudes $(u_{\rm m})$ for the first story of the structure. A larger value of $k_{\rm eff}/k_{01}$ indicates a greater increase in the overall structure stiffness due to the contribution of the real part of the complex stiffness of the damper-brace component. For a structure with a given story drift amplitude, $k_{\rm eff}/k_{01}$ increases with the increasing of the loading frequency



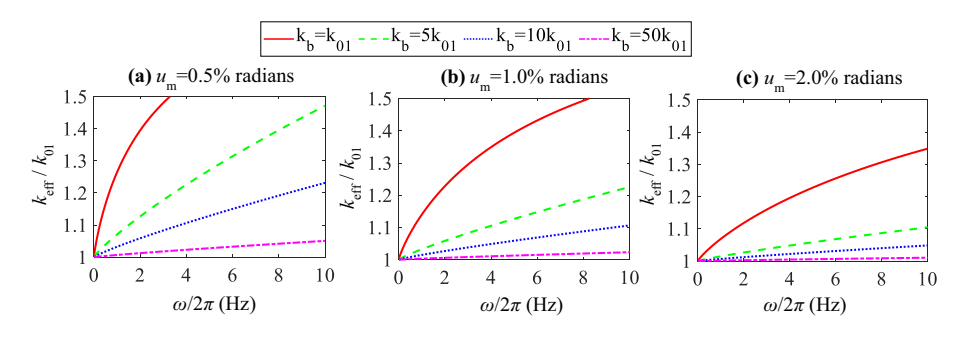


Fig. 21 Effect of brace stiffness on effective stiffness of structure with nonlinear viscous dampers

and decreases with the decreasing of brace stiffness. For a structure subjected to harmonic displacement loading with a given story drift amplitude, the ratio of $k_{\rm eff}/k_{01}$ increases with an increase in loading frequency. Increasing the brace stiffness, e.g., from $k_{\rm b}=k_{01}$ to $k_{\rm b}=10k_{01}$ substantially reduces the ratio of $k_{\rm eff}/k_{01}$ over the entire range of loading frequency. For a structure with identical brace stiffness, $k_{\rm eff}/k_{01}$ decreases with an increase in story drift amplitude. For a structure with rigid brace (i.e., $\alpha_{\rm b}=k_{\rm b}/k_{01}\to\infty$), $k_{\rm eff}/k_{01}$ approaches 1.0, which suggests the effects of complex stiffness of the damper-brace component is less significant for a structure with stiffer braces.

The variations of the normalized first mode period $(T_{\rm eff}/T_0)$ of the structure versus the loading frequency $(\omega/2\pi)$ for specified story drift amplitudes $(u_{\rm m})$ are shown in Fig. 22. As illustrated, the shortening of the period increases as the loading frequency increases, and the shortening under a smaller story drift amplitude is more obvious than that under a larger story drift amplitude. For a specified brace stiffness $k_{\rm b}=5k_{01}$ for instance, as the story drift amplitude increases from 0.5 to 2.0% radians, $T_{\rm eff}/T_0$ increases from 0.94 to 0.98 at a loading frequency of 1.0 Hz while increases from 0.83 to 0.95 at a loading frequency of 5.0 Hz. For this reason, the periods of the structure with nonlinear viscous dampers are variable rather than predetermined, due to the effect of the complex stiffness of the nonlinear viscous dampers in the structure under dynamic loading. The range of variation of the periods of the structure depends on the brace stiffness as well as the loading frequency and amplitude.

Figure 23 shows the effects of brace stiffness on the effective damping ratio ξ_{eff} over a range of loading frequency $(\omega/2\pi)$ for the structure with different story drift amplitude

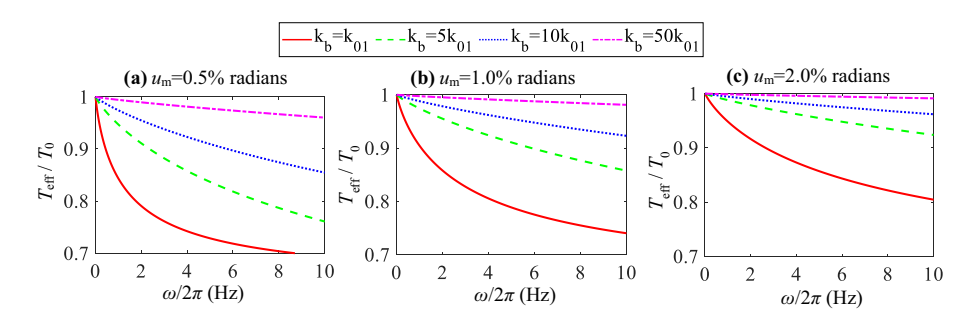


Fig. 22 Variation of structural period with respect to frequency at different story drift amplitudes

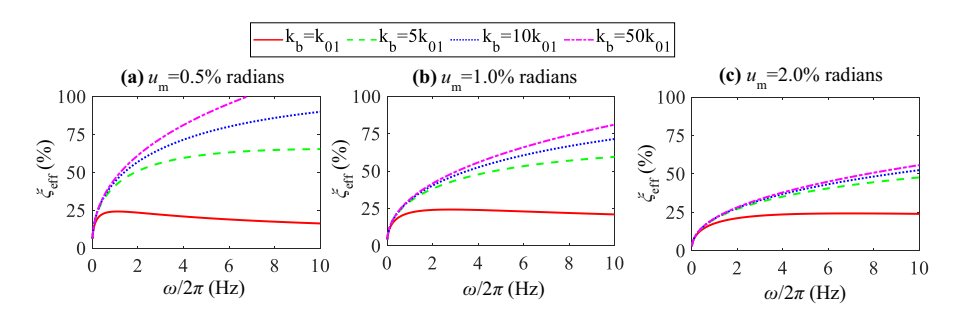


Fig. 23 Effect of brace stiffness on equivalent damping ratio of structure with nonlinear viscous damper

 $(u_{\rm m})$. It can be seen that: (1) the effect of brace stiffness on $\xi_{\rm eff}$ is more significant for a smaller story drift amplitude, e.g., with the increase of brace stiffness, the increase in $\xi_{\rm eff}$ under the story drift amplitude of 0.5% radians is greater than that under the story drift amplitude of 2.0% radians; (2) the effect of brace stiffness on $\xi_{\rm eff}$ diminishes with the decreasing of the loading frequency, e.g., the effective damping ratios are nearly the same for the structure with story drift amplitude of 1.0% radians when the loading frequency is less than 2.0 Hz and $k_b \ge 5k_{01}$; (3) a higher effective damping ratio can be achieved for a loading with higher frequency and lower amplitude, e.g., an effective damping ratio of 50% can be achieved for the structure under the loading with frequency of 5.0 Hz and story drift amplitude of 0.5% radians when $k_{\rm b} \ge 5k_{01}$; and (4) the effect of brace stiffness on $\xi_{\rm eff}$ is more pronounced for flexible braces, e.g., a flexible brace stiffness with $k_b = k_{01}$ caps the maximum level of damping that can be added to the structure over the entire loading frequency range, thereby, limiting the efficiency of the dampers in the structure. As a result, the effect of brace stiffness on damping ratio of a structure is not predetermined, rather it quantitatively depends on the frequency and amplitude of the dynamic loading that the structure is subjected to. A satisfactory design of the damper-brace components for structures with nonlinear viscous dampers is required to enable specified performance objectives to be met. Overall, a design with stiffer brace will increase the effectiveness of the damper-brace component in providing an effective damping ratio for a structural system. For instance, as indicated in Fig. 23, for a structure subjected to dynamic loading with a loading frequency equal to the fundamental frequency of the structure, a brace design with $k_{\rm b} = 10k_{\rm 0.1}$ enables compelling efficacy of the dampers in adding damping for various story drift amplitudes ranging from 0.5% to 2.0% radians.

7 Summary and conclusions

This paper presented the hysteretic damper force—deformation responses of large-scale nonlinear viscous dampers from characterization tests. The obtained damper response showed elastic flexibility exists in the damper body and clevis connection that connect the damper to the test setup. Due to the effect of the elastic flexibility, the damper force—deformation response is not purely viscous, in terms that damper force—deformation hysteretic loops have inclinations and the damper force—velocity hysteretic loops have inflations. A *nonlinear Maxwell* model was proposed for modeling the damper response. The *nonlinear Maxwell* model, which consists of a nonlinear elastic spring and a nonlinear dashpot



connected in series, was validated to provide simulated damper response that match well with the damper response obtained from the characterization tests.

An equivalent linearization of the damper response of a nonlinear viscous damper and associated elastic flexibility in the damper force path was also presented. The linearization used an equivalent linear elastic-viscous model that includes a linear elastic spring and a linear viscous dashpot. Using the equivalent linear elastic-viscous model, the effects of the elastic flexibility of brace (i.e., brace stiffness) on the effective stiffness and equivalent damping ratio of a SDOF system was investigated. Results showed that a more flexible brace (i.e., more flexible damper force path) is more likely to increase the stiffness and decrease the equivalent damping ratio of the system.

In conclusion, the study in this paper shows: (1) the elastic flexibility in the damper body and the components in the complete damper force path (such as braces, brace extensions, gusset plates, clevises, connections, etc.) have remarkable effects on damper response, which causes the non-purely viscous behavior of large-scale nonlinear viscous dampers; (2) the *nonlinear Maxwell* model provides reliable prediction of damper force—deformation response for nonlinear viscous dampers with or without associated elastic flexibility; (3) the equivalent linearization of nonlinear viscous damper response includes the effects of the elastic flexibility on damper response and enables simplified seismic design of structures with nonlinear viscous dampers; (4) a brace stiffness of greater than five times of the story stiffness (i.e., $k_b \ge 5k_{01}$) is encouraged to use in practice to compromise the effects of elastic flexibility on the effective stiffness and equivalent damping ratio of the structure.

Acknowledgements The National Science Foundation under the George E. Brown, Jr. Network for earthquake engineering simulation research (NEESR) program is acknowledged for a grant (Award No. CMS-0936610) to support the experimental work performed at the NHERI Lehigh University Real-Time Multi-Directional (RTMD) earthquake simulation facility. The analytical work reported in this paper was performed by the first author and supported by grants from the National Natural Science Foundation of China (Award No. 52078385) and the Science and Technology Commission of Shanghai Municipality (Pujiang Program: 20PJ1414000). The opinions, findings, and conclusions expressed in this paper are those of the authors and do not necessarily reflect the views of those acknowledged here.

Data availability The data used in the manuscript are available upon request.

Declarations

Conflict of interest The authors declare that there is no conflict of interest.

References

ASCE (2016) Minimum design loads for buildings and other structures (ASCE/SEI 7–16). American Society of Civil Engineers, Reston, VA

Building Seismic Safety Council (BSSC) (2009) NEHRP Recommended Seismic Provisions for New Buildings and Other Structures: FEMA P-750/2009 Edition. Federal Emergency Management Agency, Washington, DC

Chen YT, Chai YH (2011) Effects of brace stiffness on performance of structures with supplemental Maxwell model-based brace–damper systems. Earthquake Eng Struct Dynam 40(1):75–92

Christopoulos, C. and Filiatrault, A. (2006). Principles of passive supplemental damping and seismic isolation. IUSS Press.

Dong B, Sause R, Ricles JM (2016) Seismic Response and Performance of a Steel MRF Building with Nonlinear Viscous Dampers under DBE and MCE. J Struct Eng. https://doi.org/10.1061/(ASCE)ST. 1943-541X.0001482,04016023



- Dong B, Sause R, Ricles JM (2018) Seismic Response and Damage of Reduced-Strength Steel MRF Structures with Nonlinear Viscous Dampers. J Struct Eng 144(12):04018221
- Dong, B. (2016). Large-scale experimental, numerical, and design studies of steel MRF structures with non-linear viscous dampers under seismic loading. PhD Dissertation, Lehigh University, Bethlehem, PA.
- Fan, C.P. (1998). Seismic analysis, behaviour, and retrofit of non-ductile reinforced concrete frame buildings with viscoelastic dampers. Ph.D. Dissertation, Department of Civil and Environmental Engineering, Lehigh University, Bethlehem, PA.
- Fu Y, Kasai K (1998) Comparative study of frames using viscoelastic and viscous dampers. J Struct Eng 124(5):513–522
- Lee K-S, Fan C-P, Sause R, Ricles J (2005) Simplified Design Procedure for Frame Buildings with Viscoelastic or Elastomeric Dampers. Earthquake Eng Struct Dyn 34(10):1271–1284
- Lehigh RTMD Facility (2014). Lehigh RTMD Users Guide (2014). https://www.rtmd.lehigh.edu/resources/users-guide.
- Lin W, Chopra A (2003) Earthquake Response of Elastic Single-Degree-of-Freedom Systems with Nonlinear Viscoelastic Dampers. J Eng Mech 129(6):597–606
- Sause R, Hemingway G, Kasai K (1994) "Simplified Seismic Response Analysis of Viscoelastic-Damped Frame Structures", Proceedings, Fifth U.S. National Conf Earthquake Eng EERI 1:839–848
- Singh MP, Verma NP, Moreschi LM (2003) Seismic analysis and design with Maxwell dampers. J Eng Mech 129(3):273–282
- Soong TT, Spencer BF (2002) Supplemental energy dissipation: State-of-the-art and state-of-the-practice. Eng Struct 24(3):243–259
- Symans MD, Charney FA, Whittaker AS, Constantinou CMC, Kircher A, Johnson MW, McNamara RJ (2008) Energy dissipation systems for seismic applications: current practice and recent developments. J Struct Eng 134(1):3–21
- Takewaki I, Yoshitomi S (1998) Effects of support stiffness on optimal damper placement for a planar building frame. Struct Design Tall Build 7:323–336

Publisher's Note Springer Nature remains neutral with regard to jurisdictional claims in published maps and institutional affiliations.

